



Static reservoir modeling using stochastic method: a case study of the cretaceous sequence of Gamtoos Basin, Offshore, South Africa

O. L. Ayodele¹ · T. K. Chatterjee¹ · M. Opuwari¹

Received: 28 July 2021 / Accepted: 15 September 2021 / Published online: 26 September 2021
© The Author(s) 2021

Abstract

Gamtoos Basin is an echelon sub-basin under the Outeniqua offshore Basin of South Africa. It is a complex rift-type basin with both onshore and offshore components and consists of relatively simple half-grabens bounded by a major fault to the northeast. This study is mainly focused on the evaluation of the reservoir heterogeneity of the Valanginian depositional sequence. The prime objective of this work is to generate a 3D static reservoir model for a better understanding of the spatial distribution of discrete and continuous reservoir properties (porosity, permeability, and water saturation). The methodology adopted in this work includes the integration of 2D seismic and well-log data. These data were used to construct 3D models of lithofacies, porosity, permeability, and water saturation through petrophysical analysis, upscaling, Sequential Indicator Simulation, and Sequential Gaussian Simulation algorithms, respectively. Results indicated that static reservoir modeling adequately captured reservoir geometry and spatial properties distribution. In this study, the static geocellular model delineates lithology into three facies: sandstone, silt, and shale. Petrophysical models were integrated with facies within the reservoir to identify the best location that has the potential to produce hydrocarbon. The statistical analysis model revealed sandstone is the best facies and that the porosity, permeability, and water saturation ranges between 8 and 22%, 0.1 mD (< 1.0 mD) to 1.0 mD, and 30–55%. Geocellular model results showed that the northwestern part of the Gamtoos Basin has the best petrophysical properties, followed by the central part of the Basin. Findings from this study have provided the information needed for further gas exploration, appraisal, and development programs in the Gamtoos Basin.

Keywords Static modeling · Valanginian sequence · Sequential Indicator Simulation (SIS) · Sequential Gaussian Simulation (SGS) · Gamtoos Basin · South Africa

Abbreviations

Ha-B1	Well used in this study
Ha-G1	Well used in this study
Ha-K1	Well used in this study
PhiNeu	Neutron-porosity model
PhiND	Density-porosity model
SGS	Sequential gaussian simulation algorithm
SIS	Sequential indicator simulation algorithm

List of Symbols

R^2	the correlation coefficient determination
$\Phi_e, \%$	Effective porosity
mD	Milli Darcy Permeability
Φ_c	Porosity cut-off
Kc	Permeability cut-off

Vic	shale cut-off
Vsh	shale volume
K	Permeability
Φ	porosity
Sw	water saturation

Introduction

The request for oil products has placed massive pressure on the search for hydrocarbons with the development of technologies to reduce the risks of hydrocarbon exploration. Thus, it is essential to build up a reservoir model as accurately as possible to calculate the reserves and determine the most up-to-date way of recovering as much petroleum as possible in an economical way. Applying integrated geological, geophysical, petrophysical, geostatistics, and reservoir engineering is essential for reservoir characterization (Zee Ma and La Pointe 2011). A static reservoir model applies geological theory to understand the architecture of varieties

✉ O. L. Ayodele
3217090@myuwc.ac.za

¹ Department of Earth Science, University of the Western Cape, Cape Town, South Africa

of fluid flow and obstacles within the reservoir. It demonstrates the reservoir network based on information from different sources such as seismic, core, and well logs data (Viste 2008; Cannon 2018).

3D static reservoir modeling of a reservoir using seismic and well log data is an essential strategy for oilfield development. It provides insights into the prediction of reservoir performance and production (Abdel-Fattah et al. 2018). A realistic 3D static reservoir model comprising a network of faults and horizons provides the basis for model refinement integration with well data to estimate hydrocarbon accumulation and production (Abdel-Fattah and Tawfik 2015; Elamri and Opuwari 2016; Eruteya et al. 2018). The result of a robust 3D reservoir model is the representation of the reservoir in three dimensions for an efficient volumetrics calculation, uncertainty analysis, flow simulations, and well planning (McLean et al. 2012). However, a static reservoir study built from well and seismic data is mainly of non-changeable rock properties such as the lithology, clay volume, porosity, water saturation, and permeability and does not present the fluid flow behavior (Cannon 2018; Abd El-Gawad et al. 2019). Nevertheless, researchers have successfully utilized seismic and well-log data to establish a 3D reservoir model of oil and gas fields (Okoli et al. 2021). However, well log data do not individually describe the variations in reservoir petrophysical properties due to the heterogeneity nature of reservoirs, and also the well data are scattered, whereas three-dimensional seismic models thus provide an excellent description of reservoirs (Bagheri et al. 2013; Kyi et al. 2014; Amoyedo et al. 2016; Zare et al. 2020; Opuwari et al.

2021). Therefore, the proper integration of seismic data with a well log will enhance the lateral description of reservoirs.

Sequential Gaussian simulation (SGS) and Sequential indicator simulation (SIS) algorithms are often used to predict the distribution of reservoir properties. The SGS estimates the standard deviation and mean of a variable at the grid node and represents the variable at each node as a random variable with a standard Gaussian distribution (Bohling 2005). While the SIS uses indicator kriging to build a discrete cumulative density function to assign nodes to a category selected at random from the discrete cumulative density function (Bohling 2005). Thus, this present study is focused on the evaluation of the reservoir heterogeneity by integrating 2D-seismic data, well-log, and geological information objectively to generate 3D static reservoir modeling within the early Cretaceous Valanginian stage for a better understanding of the petrophysical spatial distribution of discrete and continuous reservoir properties such as porosity, permeability, and water saturation.

Geological setting

Gamtoos is an echelon twin is along with the Algoa sub-basin of the Outeniqua Basin (Fig. 1) is a simple half-graben feature controlled by the Gamtoos' fault extending deep into the crust (McMillan et al. 1997). The onshore parts of the Gamtoos fault have a throw of about 3 km, while offshore, the throw increases to about 12 km (Thomson 1999). Major tectonic movements in the offshore Gamtoos Basin occurred on the eastern flank of the St. Francis arch. In the offshore

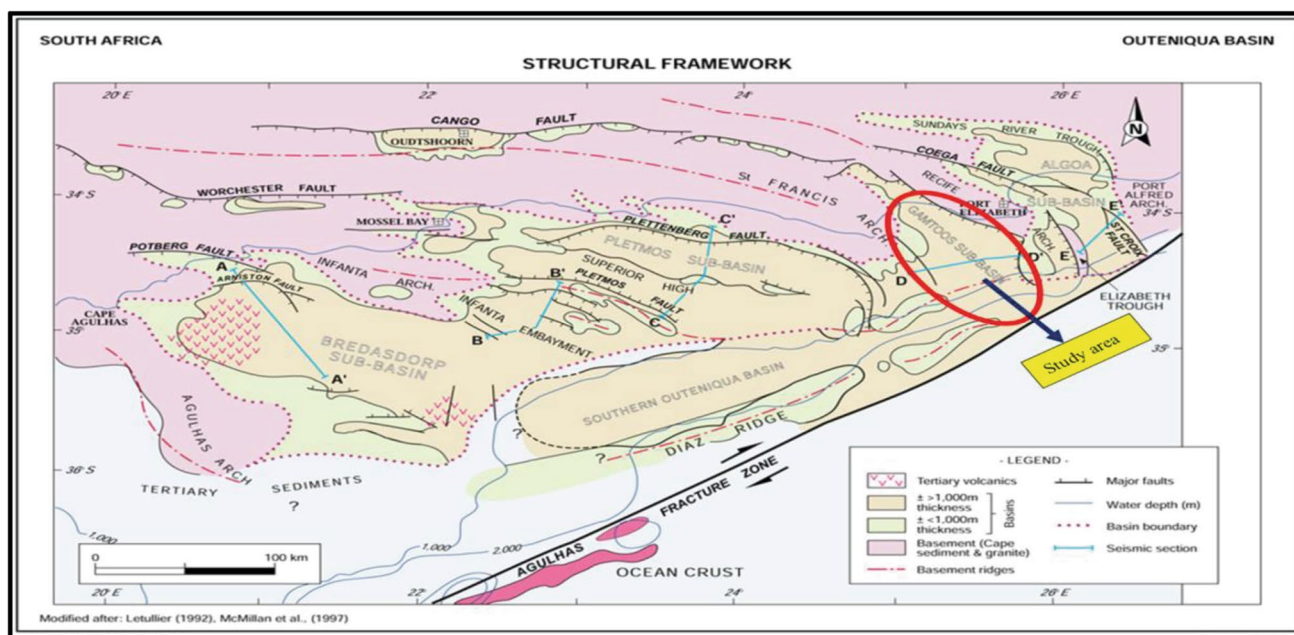


Fig. 1 Location map of the study area in the red circle, Gamtoos Basin. (modified after McMillan et al. (1997))

Port Elizabeth and Uitenhage troughs top of the basement (Horizon D reached depths of 6.5 km and 8 km, respectively). Along the southern coastline of the Western Cape and Eastern Cape Provinces on the Eastern edge of the continental shelf is the Agulhas bank with water depths of less than 200 m increasing rapidly beyond 500 m in the south at the present-day shelf edge due to the erosion caused by the Agulhas current flowing along the south-westward in the shelf edge (Malan 1993; Broad et al. 2006). The reservoir sandstones in the Gamtoos Basin mainly occur as shallow marine sandstones in the Kimmeridgian (late Jurassic) stage in the western part of the Basin and the Late Valanginian

sequence of the Basin (Fig. 2). The Valanginian sandstone sequence shows the potential for hydrocarbon exploration (Malan 1993) and deposited within the continental shelf to a deep marine depositional environment (Ayodele et al. 2020). Also, numerous stacked gas-charged submarine sandstone fans defining a Kimmeridgian to Berriasian age reservoir were interconnected in the southern parts of the Gamtoos Basin. The offshore part of the Gamtoos Basin is located along with the other echelons of Outeniqua Basin, South Africa, with reservoir sand indicating a normal pressure with no overpressure zones (Ayodele et al. 2016; Ayodele et al. 2020).

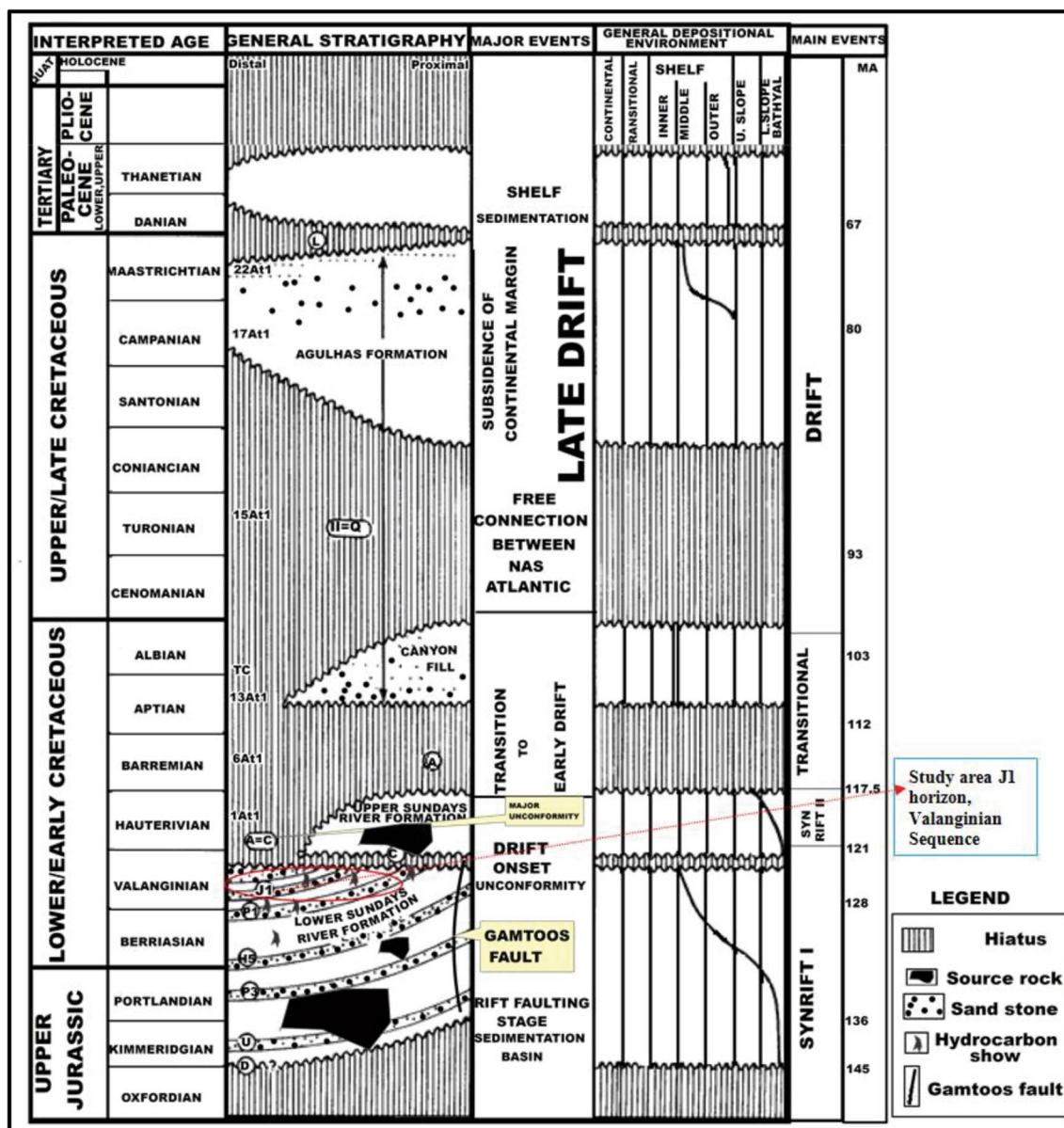


Fig. 2 Chronostratigraphic chart of Gamtoos Basin showing major unconformities, depositional sequences distribution of sandstone, source rocks, and hydrocarbon shows, the time of the events that

influence the developments of the basins, Soekor (1994) and adapted & modified after McMillan et al. (1997)

Materials and methodology

In this study, the Petroleum Agency of South Africa (PASA) provided the datasets used, which includes geological (well completion reports, conventional core analysis report, and geophysical (2D-Seismic in SEG-Y format, check shot, Navigation, and well logs (LAS format) data. The six wells used in these studies are well Ha-B2, Ha-K1, Ha-I1, Ha-G1, Ha-A1, and Ha-N1. A database was created in Petrel 2014, and Interactive Petrophysics (IP 4.2) was quality control, and editing was first performed before data processing and analysis. The structural interpretation was performed from seismic data utilizing structural modeling, creating a skeleton or a 3D reservoir network. This process was used to perform fault modeling, horizon picking, geocell network or grid cell, and layering of the 3D interpretation of seismic data. The static reservoir modeling was carried out by integrating both petrophysical and seismic data. The essential petrophysical evaluation was performed, including determining the clay volume, porosity, water saturation, and permeability from well logs. The core data were used to calibrate the well log measurements. The determined petrophysical properties were used as an input parameter for upscaling. The upscaled logs were used for geocell Modeling and variogram distribution. In this study, petrophysical parameters are simulated using the Sequential Gaussian Simulation (SGS) algorithm. In contrast, the lithofacies architecture is simulated using the Sequential Indicator Simulation (SIS) algorithm to control the model distribution of the reservoir's petrophysical properties (porosity, permeability, and water saturation) since they are closely related. The reservoir structural model shows no significant faults around the well's location of the study area except minor listric faults. The flowchart adopted in this study is shown in Fig. 3.

Results and discussion

Seismic interpretation

In this study, seismic data interpretation was carried out to image subsurface structures (Yilmaz 2001). The most important step taken in interpreting seismic data was to create the relationship between the seismic reflection and stratigraphy of the area. The correlation between the borehole data and the seismic data enables identifying and correlating the seismic horizon with the formations. To perform the seismic modeling for this study, depth conversion was carried out. The seismic data recorded in

the time domain was converted to depth domain because the well data was utilized for the study area in the depth domain. The density and sonic logs of six exploratory wells, Ha-B2, Ha-K1, Ha-I1, Ha-G1, Ha-A1, and Ha-N1, were calibrated with check shot data to perform the well (depth,m) -to-seismic (time, milliseconds) ties, to link stratigraphy to seismic reflection (Avseth et al. 2010) and to generate the synthetic seismogram. The results from the seismic well tie processing are presented in Fig. 4.

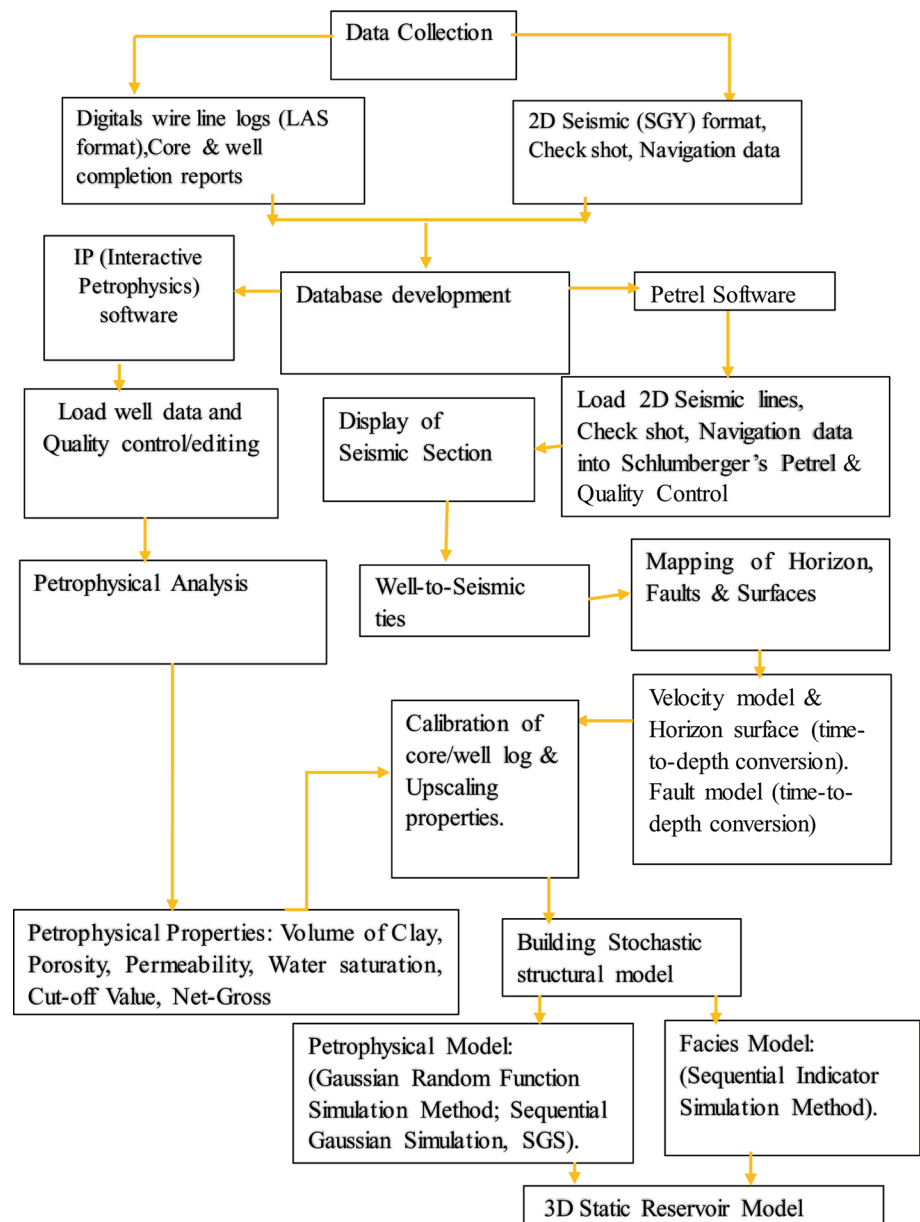
For the static reservoir modeling of this study, the first step was to interpret seismic data, which were performed by interpreting the seismic horizons using geological information and geophysical methods. Then, the geophysical methods were used to compare the seismic traces with the synthetic seismogram at the well location. The process enabled accurate mapping and picking of horizons. Thus, the Valanginian reservoirs surfaces (J1, horizons) and some minor listric faults in the reservoir layers were picked across the six wells Fig. 5a, b presents the surfaces created from the reservoir at horizons J1 for time and depth domains.

The structural model of the Valanginian section of this study was based on seismic interpretation data. The created horizon and fault surfaces are the main components of the structural model. Most of the faults mapped on seismic reflection data of the Valanginian sections are minor listric faults that have no specific significance to the model, and erosional events formed as a result of tectonic uplift occurred in the area. These faults are located at the central portion of the Valanginian section trending North–South (Fig. 6). The sediments are thinned out based on tectonic action, which ranges from 0 m to – 1.5 km thickness from the northeast toward the southern part of the study area. The sedimentation in the North-West to the Southwestern part of the study area developed thickness sediments ranging from approximately 2.25–3 km. No significant fault was observed. The absence of a significant fault in the area may be one of the reasons for the absence of hydrocarbon fill mechanism of the formation in the wells across the section.

Structural modeling and creation of polygon

Structural reservoir modeling is the first step in static reservoir modeling that includes seismic interpretation of the geological horizons, faults, and geocellular network are vital in static reservoir modeling (Rahimi and Riahi 2020). This model forms a 3D geometric framework and determines the range of petrophysical models (Canon 2018). Thus, a simple 3D geometric grid process was performed in this study to create cell grids containing the reservoir's geometry to denote the geological and petrophysical reservoir properties, respectively, due to the 2D seismic data used in this study which does not support the 3D model directly. The grid cells have an optimized increment

Fig. 3 Flowchart depicting the methodology adopted in the study



of 50 m by 50 m along X and Y direction, respectively, and limits of $561 * 718$ nodes dimension. The created 2D horizon surfaces recorded in time were converted to surface depth, moved into the structural framework, and converted to simple 3D grids through structural gridding. This process enables the discrete populating of the facies and petrophysical property values into the grid cells to characterize the geometry. The grid cells were oriented in the north–south direction along with the well’s position and the 3D grid mode. The geocellular network is shown in Fig. 7. A polygon was created to cover the seismic horizons mapped from the 2D line-seismic data based on the formation tops. This process was later used to model the surface generated for this study.

Petrophysical analysis

Before the petrophysical analysis, a well log lithology correlation between the studied wells using formation tops and gamma-ray was first applied to identify facies. A gamma-ray log baseline of 80,120 api to represent different facies were used. An interval with ≤ 80 api represents sandstone, an interval having 80 to 120 api represents siltstone, while an interval having readings of ≥ 120 api represents shale. As a result, three different facies were identified as sandstone, silt, and shale (Fig. 8). This process enabled well-to-well correlation, defined the stratigraphic horizons bounding the main geological sequence, and observed the facies variation in the main reservoir J1 horizon.

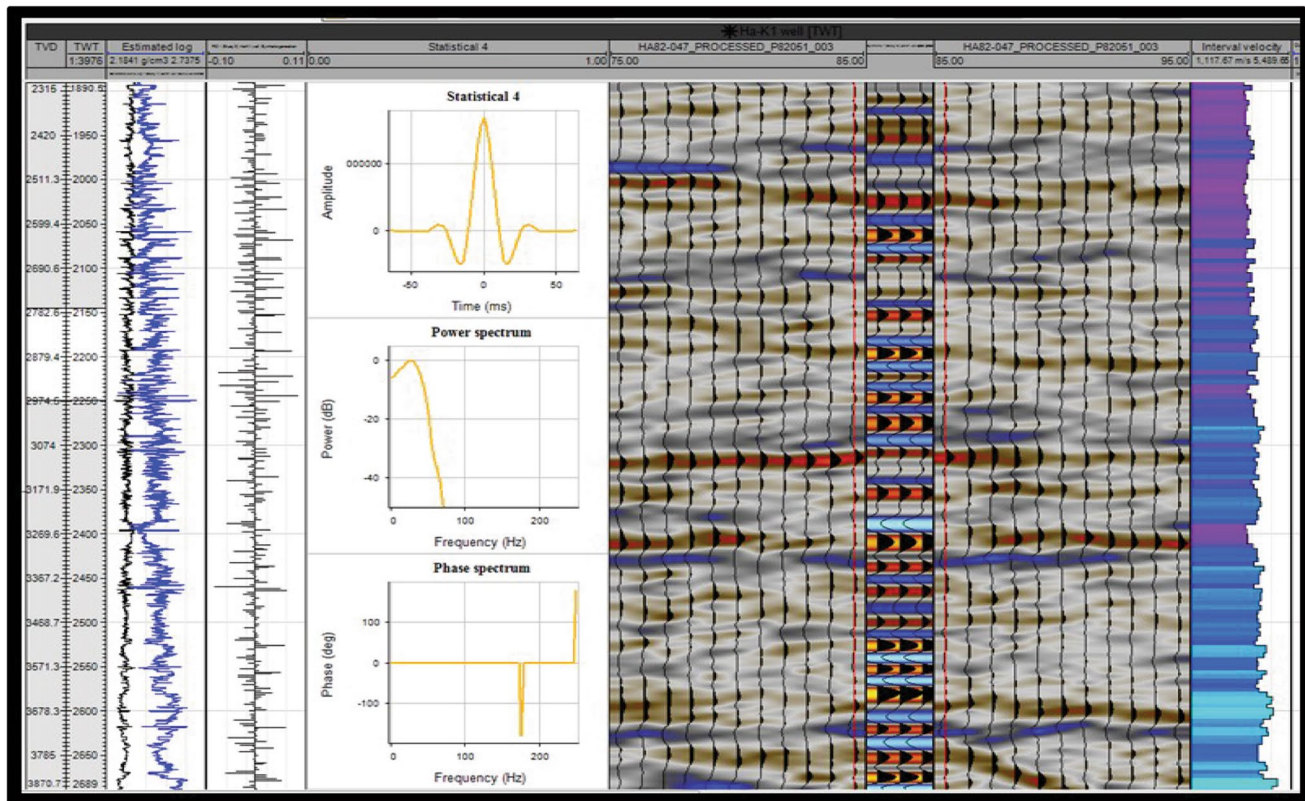


Fig. 4 The results from the seismic well tie processing

The petrophysical data analysis was performed to aid the static model of the reservoirs within the Valanginian section of the studied area. The conventional suites of petrophysical well logs data such as gamma-ray, resistivity, neutron, sonic and density logs available in the six wells were analyzed using IP (Interactive Petrophysics software) to estimate the petrophysical properties, such as the volume of clay, porosity, permeability, and water saturation. The volume of shale was obtained from the gamma-ray log using the linear formula (Asquith and Gibson 1982), and then corrected for shaliness using the nonlinear Larionov method for older rock:

$$IGR = \frac{Gr \log - Gr \min}{Gr \max - Gr \min} \quad (1)$$

$$Vsh = 0.33 (2^{(2 * IGR)} - 1) \quad (2)$$

where IGR (decimal) is the gamma-ray index (decimal), Grlog (api) is the gamma-ray log reading of the formation, Grmin (api) is the minimum gamma-ray log reading, and Grmax is the maximum gamma-ray log reading (Atlas, 1979). The calculated IGR in Eq. 1 was used in Eq. 2 to calculate the shale volume (Vsh) using the Larionov method (Larionov 1969).

At the same time, the total porosity was estimated from the density log using an average matrix density value of 2.67 g/cm^3 from core grain density (Asquith and Gibson 1982; Opuwari 2010) from Eq. 3:

$$\Phi_t = \frac{\rho_{ma} - \rho_b}{\rho_{ma} - \rho_{fl}} \quad (3)$$

$$\text{Effective porosity} = \Phi_t - Vsh \quad (4)$$

where ρ_{ma} (g/cm^3) is the matrix density, ρ_b (g/cm^3) density log reading, ρ_{fl} (g/cm^3) is the fluid density, and Φ_t (%) is the total porosity from the density log.

A shale volume correction was applied to density calculated total porosity (Φ_t) to obtain an effective porosity using Eq. 4. The permeability was estimated from an empirical equation obtained from the core permeability versus porosity cross plot. Water saturation was estimated from the Indonesian method by Worthington (1985) because of the high volume (an average of 38%) of silt and shale in the reservoir. Core-based petrophysical property results were available. All log estimated measurements were validated and calibrated with direct core measurements results from the petrophysical evaluation were upscaled. A cross plot of petrophysical properties of effective porosity, permeability,

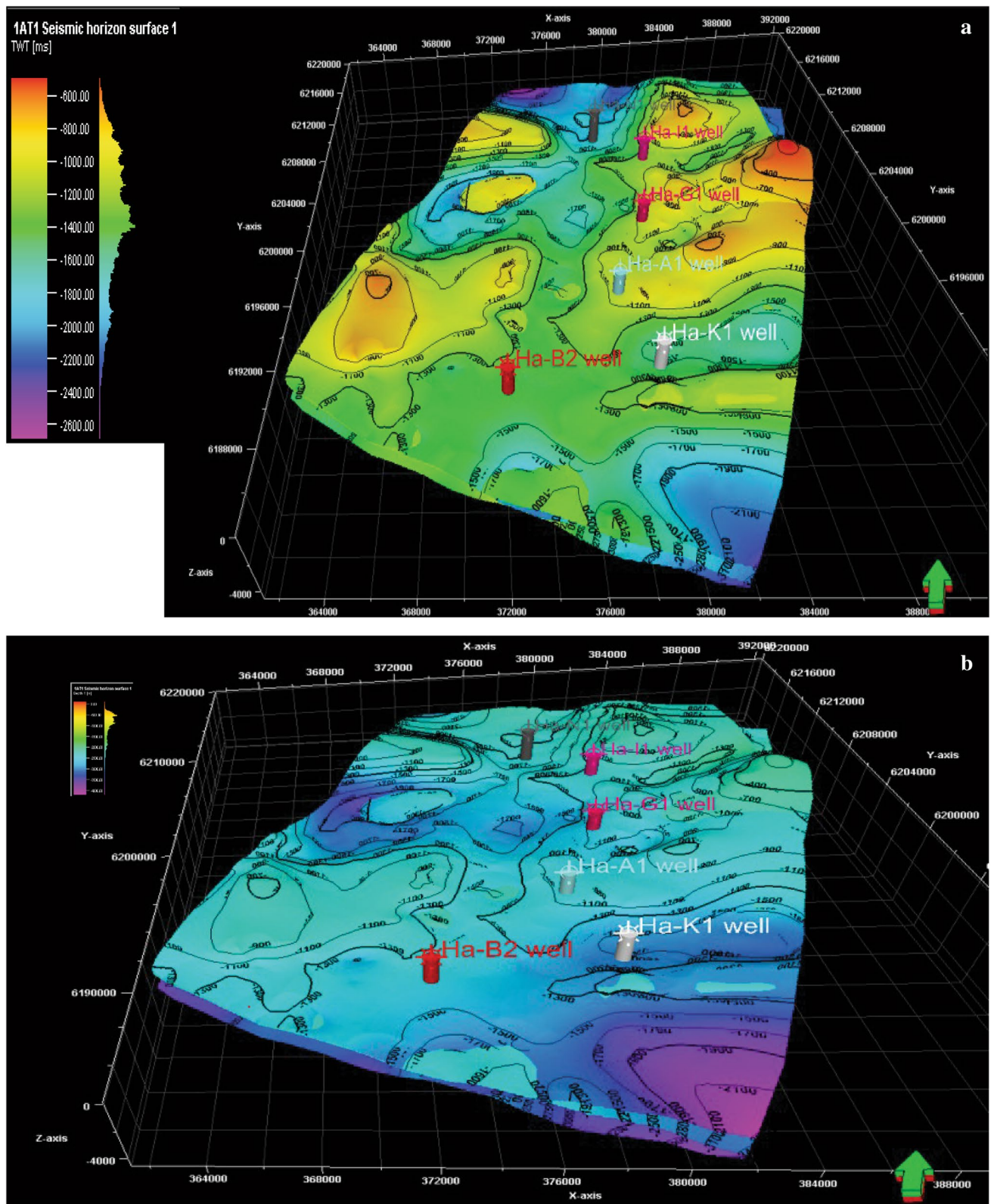


Fig. 5 a Result of horizon surfaces in-time created from the horizons J1 sequence b Result of horizon surfaces in-depth created from the horizons J1 sequence

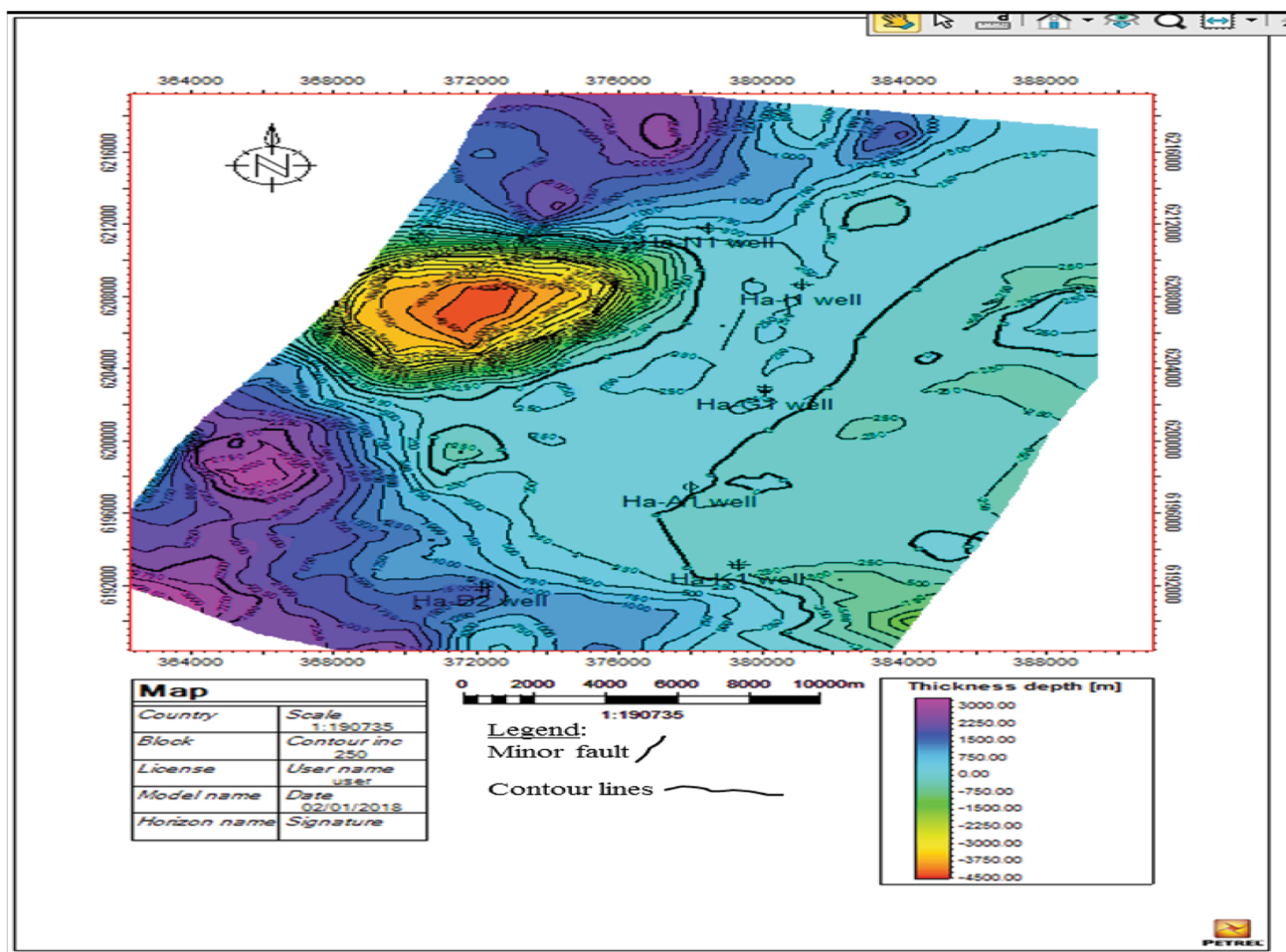


Fig. 6 Depth (m) structured thickness map model of J1 horizon (Valanginian) across the study area showing listric faults

and water saturation was performed. Consequently, effective porosity cut-off 8%, permeability cut-off of 1mD, and water saturation cut-off of 65% were used to estimate net pay intervals. The net pay refers to the interval or portion of the rock that can contain hydrocarbon (Yang et al. 2019).

Upscaling for this study aims to place the geometrical location of the petrophysical properties in each geocell. Also, the volume of data logs is very tiny, and to observe the properties in a cell, the mean of these points has to be displaced in the cell. Thus, the geocell input parameters designed in the reservoir network model for this study are evaluated by the averaging method. The averaging method by the arithmetic mean was used to upscale the additive petrophysical properties such as porosity and water saturation. The geometric mean method was adopted in upscaling the calculated permeability (K) because of its spatial correlation in the reservoir and because it is log-normally distributed and its sensitivity to lower values. The “Most of” algorithm upscale method value, being the most represented in the penetrated cells were used for the facies upscale. The

two primary constraints for upscaling are that the data have a normal distribution and no orientation in the input values (Dake 1983; Mattar and Dean 2008).

In the modeling of petrophysical parameters in the present study, the upscaling helped to populate the grid cells for stochastic simulation algorithm methods, utilizing Sequential Gaussian Simulation (SGS) method in assigning the properties. This method was adopted because it allows the modeling of properties by lithofacies, honoring the well log data, allowing input parameter distributions, producing a histogram, and providing a clear variogram and trends.

Variogram application

A variogram is a computational tool that can examine spatial data structures (Goovaerts 1992; Hazlett 1997; Rahimi and Riahi 2020). The variogram was applied in this study because the histogram alone cannot disclose the location and directional change of the distribution of reservoir properties. Therefore, the aspherical variogram model with sills

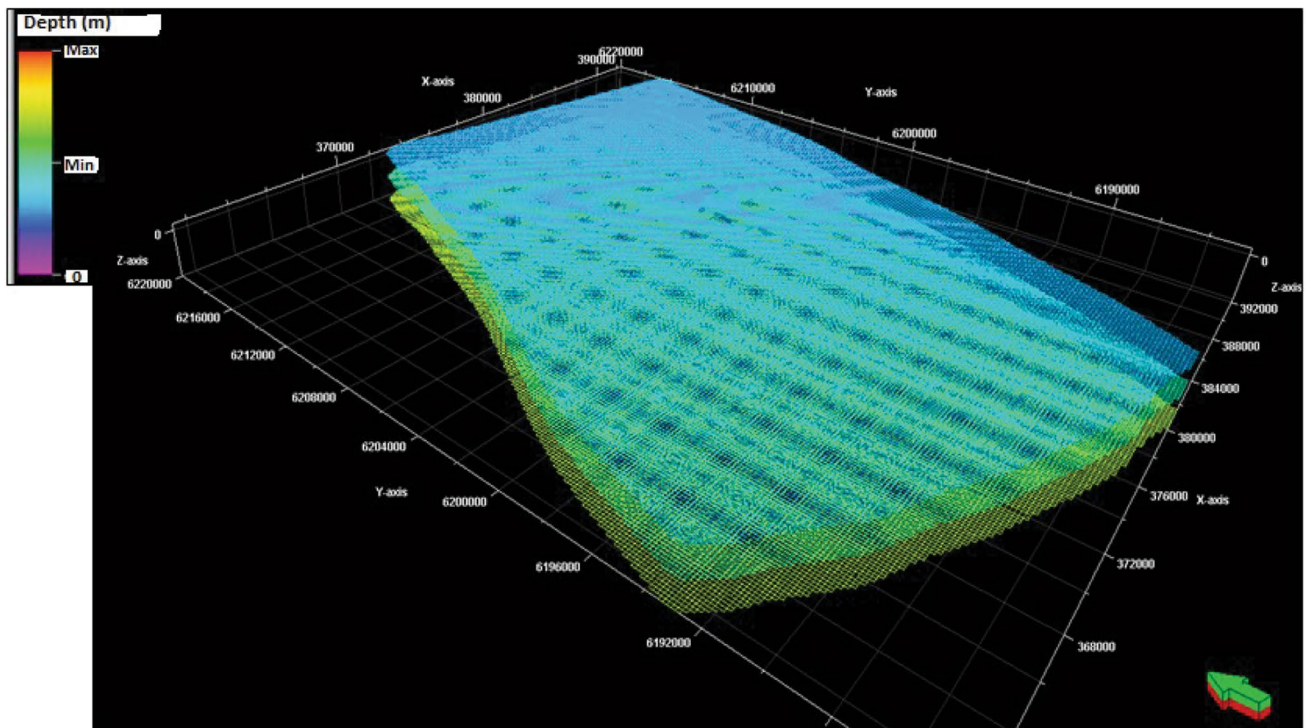


Fig. 7 The result of simple 3D cellular gridding cells ($207 \times 238 \times 21$) are built through structural gridding

known as a transition model that describes the data and serves as input into the property modeling was adopted in this study to understand the variability structure of distributed reservoir properties. Variogram data for each property upscaled were generated to identify anisotropy and direction of maximum data continuity of the Variogram model properties. The Variogram parameters values such as Sill of 1.0, Nugget of 0.0001, and anisotropy range of 14,416 of both major and minor directions. In the vertical direction for well information and area variation, an azimuth of 63° with dip 0° in a clockwise direction and spherical variogram type were all selected and applied to generate an accurate result of the Variogram model. Thus, the resultant model was used in populating the facies and petrophysical properties in the 3D grid cells using the stochastic simulation algorithm method employing the Gaussian Random Function Simulation (GRFS) algorithm modeling in this study. Figure 9 indicates a sample variogram plot (semivariance) combining neutron-porosity and water saturation generated data analysis obtained for this study.

Facies modeling

The Stochastic Simulation method using Sequential Indicator Simulation (SIS) algorithm by Kriging indicator was adopted to model facies in this study after the upscaling of the Facies log. The treat-log line and neighbor-cell method,

which enabled all penetrated cell layers relatively to their variogram distance to populate facies, was also adopted for the upscaling facies. The lithofacies were discriminately coded at the wells based on log data, primarily the gamma-ray logs (GR) available for the wells by using Python script; (Gamma Ray (GR 1) < 80 , 0, If (GR 1) > 80 GR 1 < 120 , 1, 2)). Where 0 represents sandstone, 1 represents siltstone, and 2 represents shale. The GR values less than 80 API are classified as 0 (Sandstone), GR values between 80 and 120 API are classified as siltstone, while GR values greater than 120 API are classified as shale. To simulate a discrete property (facies) for the studied area, the sequential indicator simulator (SIS) method was applied using the Kriging indicator. This algorithm was adopted because it can control an average frequency and variation of the discrete spatial continuity and enable easy modeling of facies environments. The facies volume shares vary vertically, laterally, or both. Also, it ensures to transform a continuous distribution to a discrete distribution and its drive to simulate complex facies heterogeneity (Yu and Li 2012).

Static reservoir modeling

Static modeling plays a significant role in studying a hydrocarbon reservoir by enabling the calculation of the hydrocarbon volume (Abdel-Fattah et al. 2018; Abd El-Gawad et al. 2019). This includes a geocellular network containing

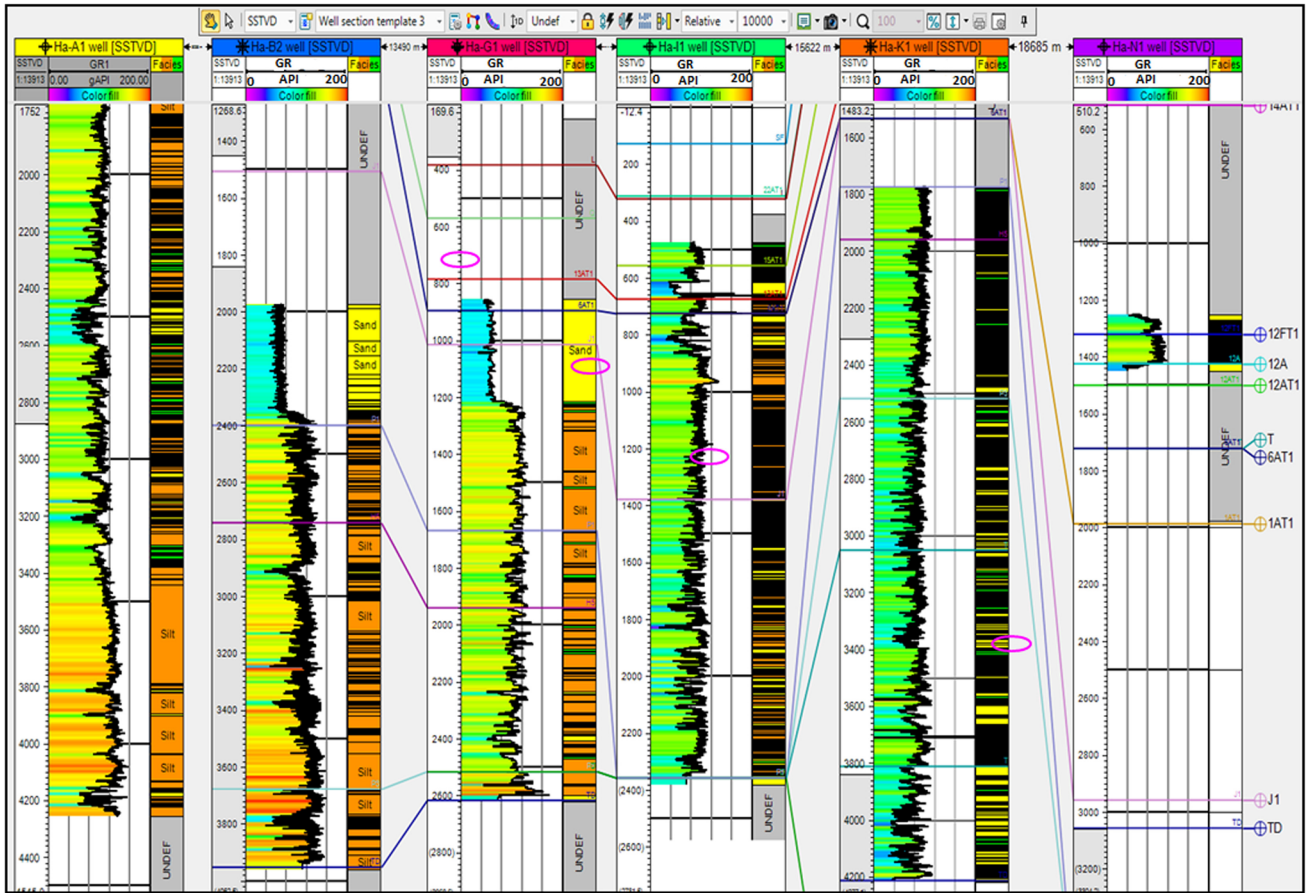
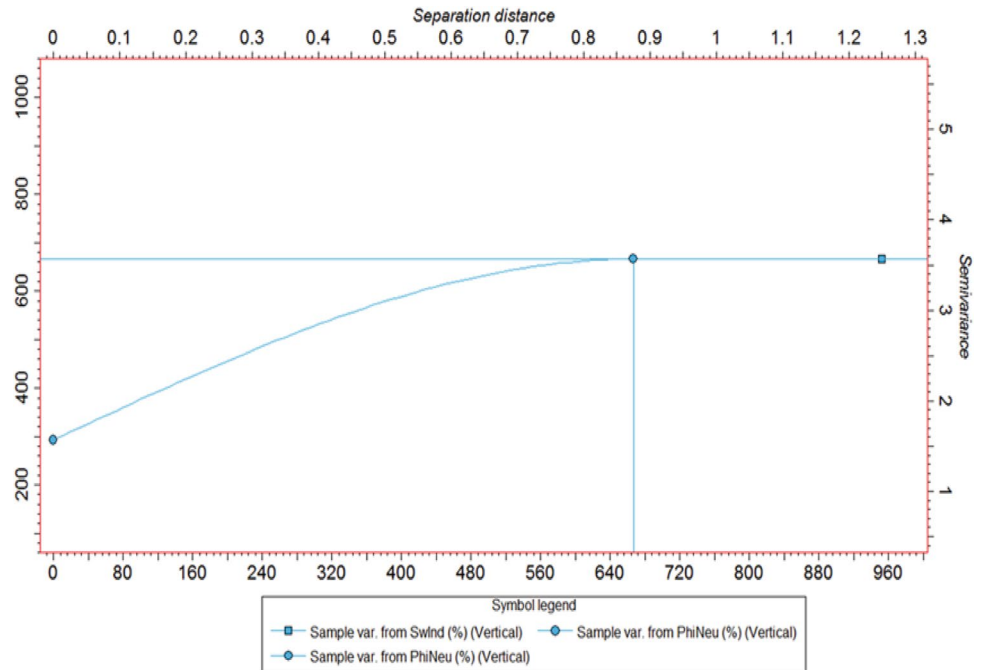


Fig. 8 Gamma-ray log well correlation between the studied wells

Fig. 9 Results of variogram (semi-variance) of porosity and water saturation generated data analysis



parameter information such as stratigraphy and faults modeling that aid in constructing the structural model and petrophysical properties. The 3D grid model, known as the geocellular model, usually has thousands to millions of geocells. As a result, the rock facies and petrophysical properties (porosity, permeability, and water saturation) can be specified (Pyrz and Deutsch 2014). In this study, to evaluate the reservoir parameters, static petrophysical modeling was simulated using the Geostatistics simulation method to generate data compatible with a spatial variable and create histograms, model spatial variability of the actual data, respectively. The Sequential Gaussian Simulation (SGS) algorithm method was adopted to provide a complete classification of the reservoir parameters continuously in each cell of the 3D network and reduce computational time and detect the reservoir anisotropy and reflect such anisotropy in the generated model. The five simulation procedures of this method duly complied within this study, viz. (a) by selecting a random point to estimate in the unknown dataset (b) application of the kriging method using the random value for the unknown

dataset and variogram method (c) selections of a random value for an unknown point (d) at this stage the simulated point is considered as the known point and used to simulate the next randomly chosen unknown point (e). Then, steps a to d, repeated for random realization to avoid unknown points. This study's rock facies (lithofacies) were simulated using the Sequential Indicator Simulation (SIS) algorithm Kriging indicator. This aids to control the model distribution of petrophysical properties within the reservoir since they are closely related. Based on the rock facies simulated in this study using the above method, the sand bodies in the formation fraction, i.e., the sand, silt, and shale contents, were 43.18%, 42.02%, and 14.79%, respectively Fig. 10.

Based on the petrophysical evaluation carried out using the above-stated method in the Valanginian section of the present Basin, the mean effective porosity logs model upscaling using arithmetic averaging methods runs variogram was calculated between 8 and 22% (Fig. 11). The mean of a geometric method upscale the calculated permeability as the spatial correlation in the reservoir is log-normally

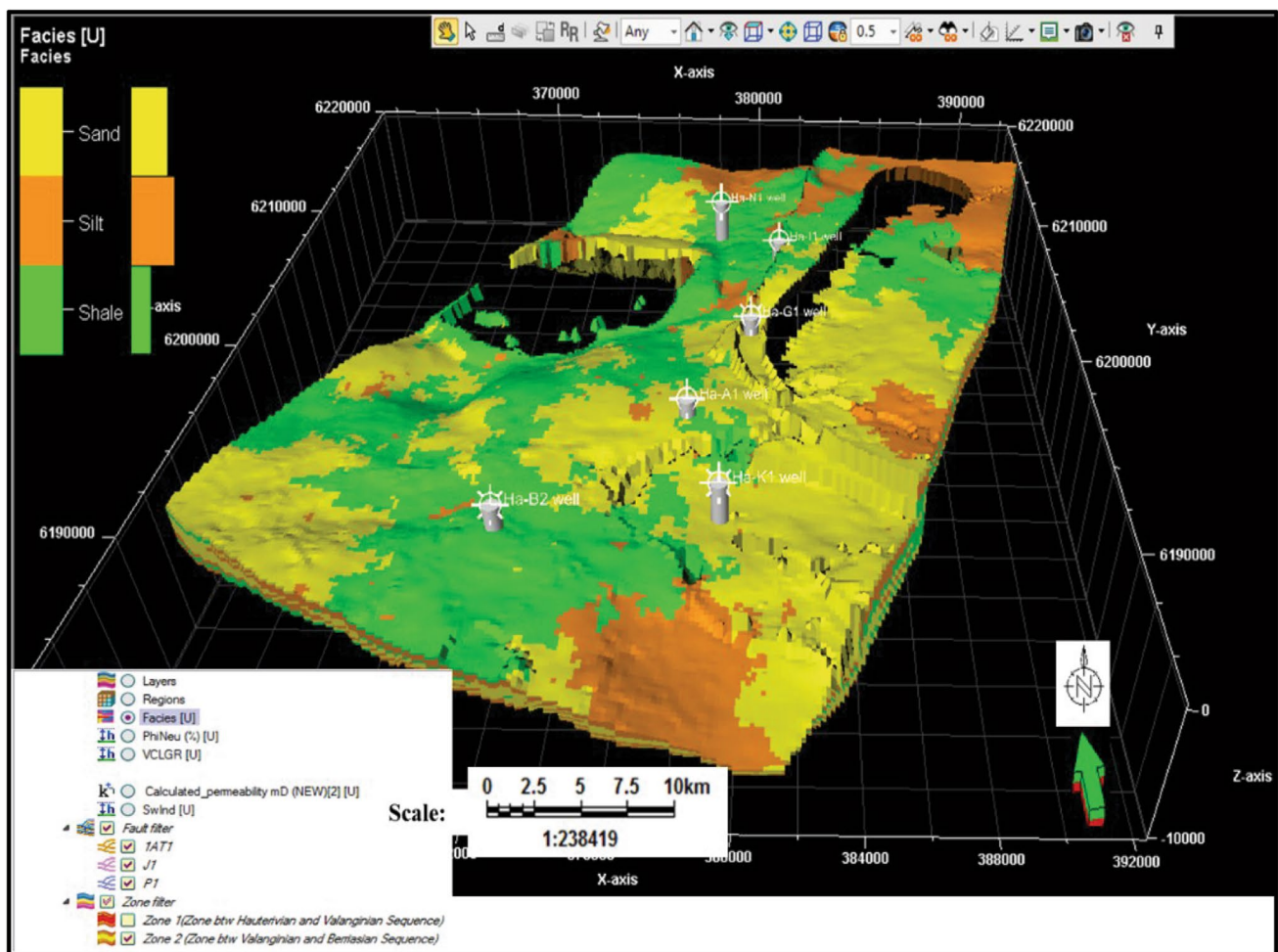


Fig. 10 Result of 3D-grid-model perspective view distribution of upscaled Lithofacies

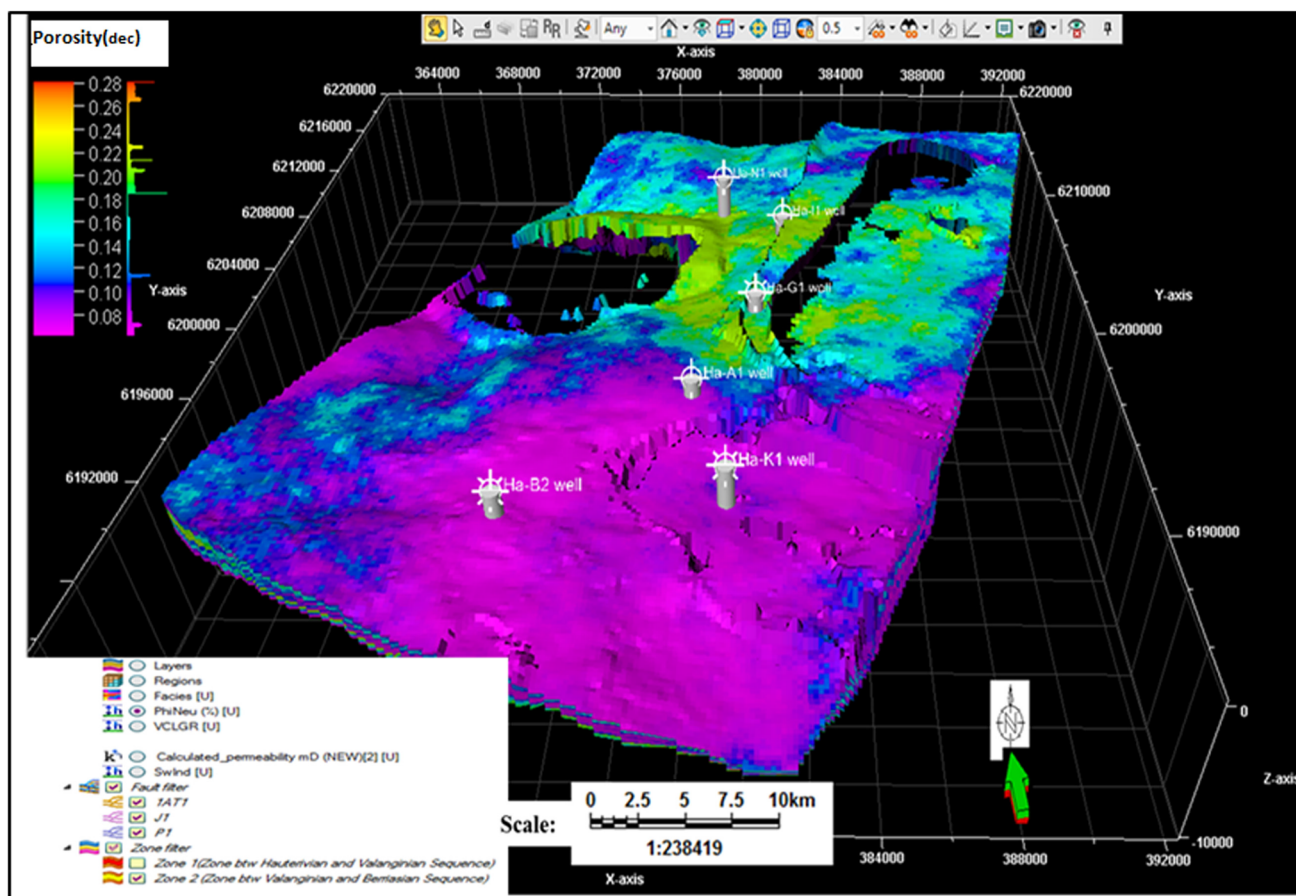


Fig. 11 Result of 3D-grid-model perspective view distribution of upscaled porosity

distributed and sensitive to lower values. The calculated permeability is mainly concentrated between 0.1 and 1.2mD within the Valanginian section (Fig. 11). While the water saturation cut-off results derived from the petrophysical interpretation were used to determine the hydrocarbon-bearing zones (pay) and water-bearing zones (wet) in the interval evaluation of the Valanginian section was 66%. The intervals with 66% or below water saturation were believed to be hydrocarbon-bearing zones, while the intervals greater than this value was considered wet or non-productive water-bearing intervals.

The 3D lithofacies surface depth attribute map (Fig. 10) indicates a mass flooding characterized by thick-bedded siltstone lobe (siltstone facies) with intercalated fine mudrock (shale facies) and minor sandstone in low energy turbidite channel environment in the southwestern part of the studied area (Flint et al. 2011). The northern part indicates a diachronous deposition dominated by sandstone, intercalated with minor siltstone and shale, probably deposited in a high energy turbidite channel, followed by low energy settling of the siltstones and shale before the next pulse of high energy sandstones were deposited (Spychala et al.

2017). The northeast to the southeast of the Valanginian section sequence suggests that high energy turbidites might be encountered. Erosional surfaces characterize the marine deposits dominated by sandstone intercalated with siltstone and minor shale due to tectonic processes resulting from uplift that created a sediment hiatus in the section (Surplus et al. 2009). In general, the distributions of the facies in Valanginian section indicate an abundance of shale facies compared to sand and silt facies. Geologically the eastern and central parts show a distribution of sand facies where reservoirs are encountered within the formation. The southwestern parts dominated by shale and sand facies; show a reservoir and good seal for hydrocarbon accumulation which can prevent spill points during the hydrocarbon migration. The study revealed that the argillaceous facies (shale) are more dominant than the good arenaceous facies (sand) in the study area. Thus, the dominance of shale lithology in the study area, based on reservoir rock quality, suggests that the Valanginian section potentially lacks good quality reservoir sand. These facies are deposited in varying depositional environments between shallow marine to deep marine of the continental

shelf, submarine fan lobes, and basin floor depositional environments.

The porosity distribution model (Fig. 11) shows a good porosity in the northcentral part of the study area and ranges between 16 and 22%, around well Ha-II, Ha-G1, and Ha-N1. This good porosity is an indication that the pore space in the reservoir sand can store fluid. However, in the southern part of the study area, the porosity distribution indicates poor to fair porosity values ranging from 8 to 10% within the Ha-B2, Ha-K1, and Ha-A1 wells. Reservoir properties, which include the porosity of tight sandstones, have an intimate relationship with depositional facies, diagenetic features,

and clay minerals(Calderon and Castagna 2007; Kashif et al. 2019). Consequently, we infer that facies, diagenetic effects, and clay mineral present may be due to the variation in the porosity distribution in the study area. This indicates that the southern part’s reservoir rock has no substantial pore space capacity to store fluids. In general, based on the average porosity value of 14% of the entire study area, the area can be classified as fair reservoir rock property based on the classification of porosity and permeability proposed by Levorsen and Berry (1967), presented in Table 1.

Table 1 Classification of reservoir porosity and permeability values (modified after Levorsen, (1967))

Porosity (%)	Classification	Permeability (mD)	Classification
0–5	Negligible	≤ 10.5	Poor to Fair
5–10	Poor reservoir rock	15–50	Moderate
10–15	Fair reservoir rock	50–250	Good
15–20	Good reservoir rock	250–1000	Very good
20–25	Very good reservoir rock	> 1000	Excellent

The upscaled 3D permeability map (Fig. 12) indicates a permeability distribution concentrated mainly between 0.1 to 1.2 mD, with the average permeability less than 1.0 mD in the entire reservoir rock. This value indicates a poor permeability, a reflection of poor connectivity pore space reservoir sand’s inability to transmit fluid. This suggests that the area under investigation has no substantial permeability within the reservoir rock. Therefore, according to a qualitative permeability evaluation, this poor-quality reservoir rock unit cannot transmit fluids.

The upscaled 3D water saturation model (Fig. 13) reveals water saturation distribution within the wells Ha-N1, Ha-II, Ha-G1, Ha-A1, Ha-K1, and Ha-B2 in the entire section varies from 30 to 85% (Fig. 13). This indicates a

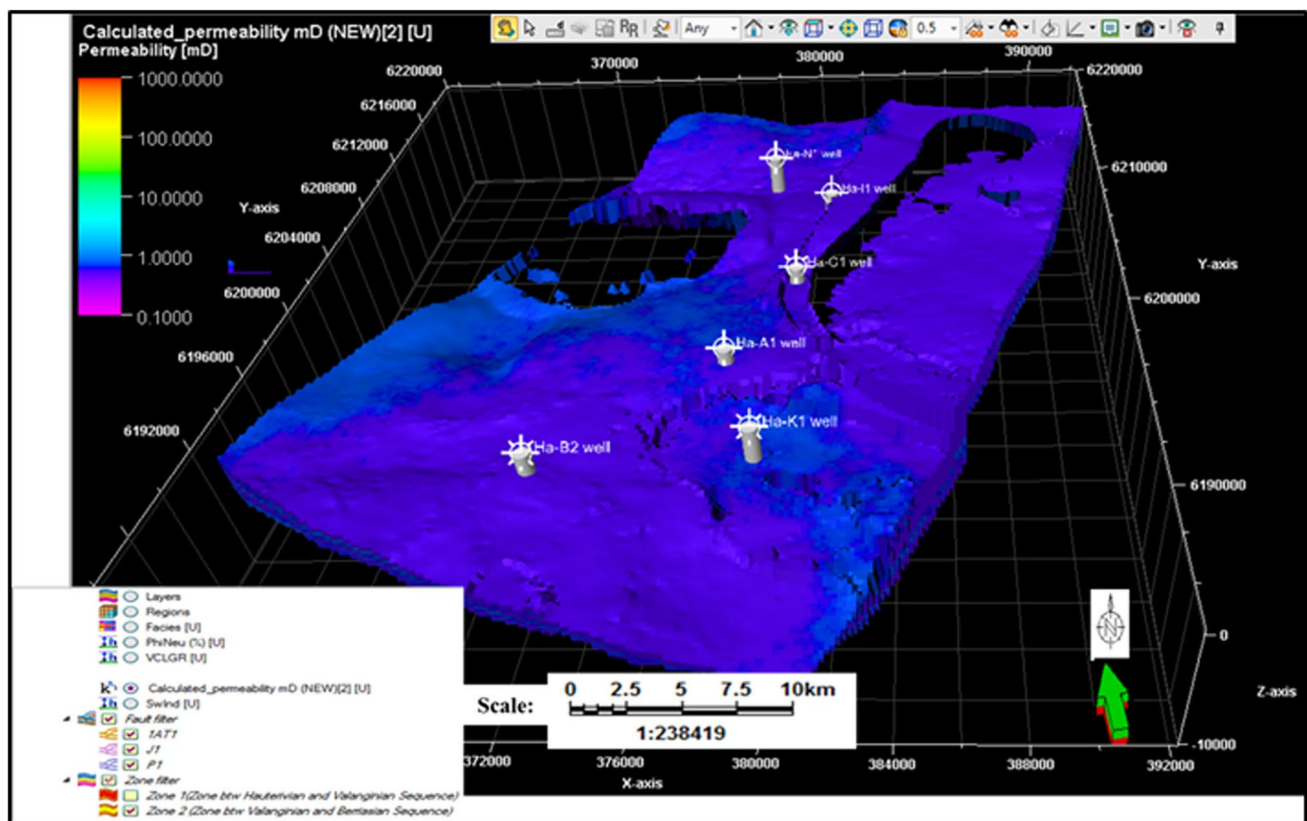


Fig. 12 Result of 3D-grid-model perspective view distribution of upscaled permeability

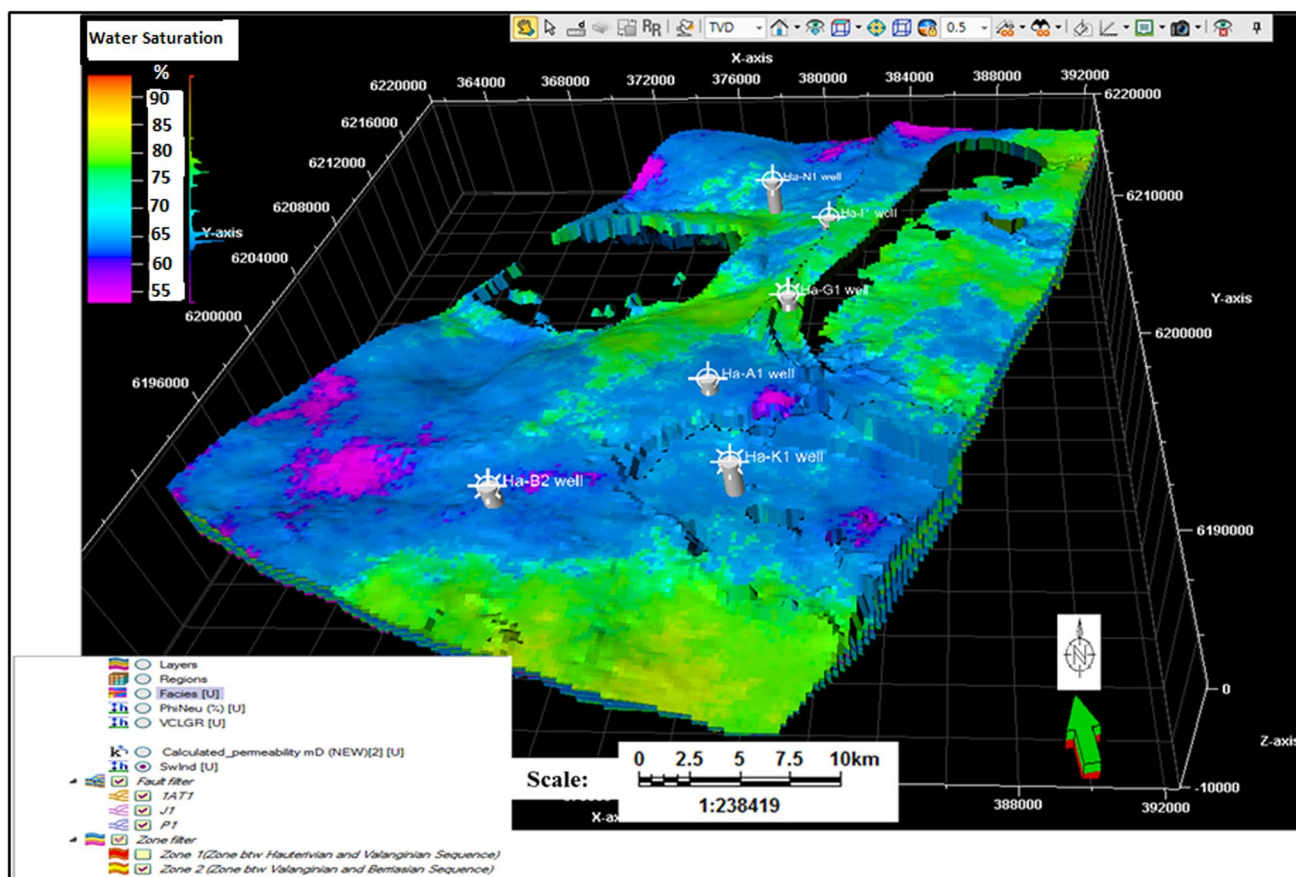


Fig. 13 Result of 3D-grid-model perspective view distribution of upscaled water saturation

hydrocarbon-bearing reservoir, suggesting that the Valanginian section can be regarded as a hydrocarbon-bearing reservoir unit. The changes in the petrophysical properties generally tend to be facies controlled because areas predominantly of shale and silt have porosity $\leq 8\%$, permeability $\leq 1\text{mD}$, and water saturation $\geq 65\%$, indicating an inability to produce hydrocarbon is observed in the northeastern and southwestern part of the study area. Whereas, areas dominated by sand in the northwestern part of the study area have porosity $\geq 8\%$, permeability $\geq 1\text{mD}$, and water saturation $\leq 65\%$, showing potential net pay.

Conclusion

This study has integrated and evaluated seismic, well log, and core data to generate information that would assist in the delineation of petrophysical properties and hydrocarbon prospect locations within the Gamtoos Basin, offshore South Africa. The study has proven to be successful in identifying the poor petrophysical properties of the formation as one of the reasons for the inability of the Gamtoos Basin to produce a commercial quantity of hydrocarbon. This

study performs static reservoir modeling for the petrophysical properties (porosity, permeability, and water saturation) using the Sequential Gaussian Simulation (SGS) method. Static reservoir modeling provides expected results using the geostatistics method in the complex geological structure of the reservoir section in the Valanginian reservoirs of the Gamtoos Basin. The evaluated petrophysical properties indicate that the reservoir porosity and permeability in the Valanginian section are concentrated between 5 and 22% and permeability ranges from 0.1 to 1.2mD (average mean permeability of $< 0.1\text{mD}$) from the north to the south across the studied area, the water saturation ranges between 30 and 85%. The distribution of petrophysical properties presented by the reservoir property maps would guide during the exploration, appraisal, and development phases of the Gamtoos Basin. Based on the constructed static geological reservoir model, the northwestern part of the Basin presents the best location for hydrocarbon prospecting. Furthermore, the results show that static modeling can improve methods for reservoir evaluation and subsurface geological studies.

Acknowledgements The authors wish to acknowledge the Petroleum agency South Africa, Cape Town office for providing data used in this

study, and the Earth Science Department of the University of the Western Cape, South Africa, to provide conducive environments for conducting this research. Also, appreciate Professor J. Van Bever Donker proofreading this research during the period of study.

Declarations

Conflict of interest Authors have declared that no competing interest exist.

Ethical approval The research does not require any ethical clearance issue.

Open Access This article is licensed under a Creative Commons Attribution 4.0 International License, which permits use, sharing, adaptation, distribution and reproduction in any medium or format, as long as you give appropriate credit to the original author(s) and the source, provide a link to the Creative Commons licence, and indicate if changes were made. The images or other third party material in this article are included in the article's Creative Commons licence, unless indicated otherwise in a credit line to the material. If material is not included in the article's Creative Commons licence and your intended use is not permitted by statutory regulation or exceeds the permitted use, you will need to obtain permission directly from the copyright holder. To view a copy of this licence, visit <http://creativecommons.org/licenses/by/4.0/>.

References

- Abd El-Gawad EA, Abdelwahhab MA, Bekiet MH et al (2019) Static reservoir modeling of El Wastani formation, for justifying development plans, using 2D seismic and well log data in Scarab field, offshore Nile Delta Egypt. *J Afr Earth Sci* 158:103546
- Abdel-Fattah MI, Metwalli FI, El Sayed IM (2018) Static reservoir modeling of the Bahariya reservoirs for the oilfields development in South Umbarka area, Western Desert Egypt. *J Afr Earth Sci* 138:1–13
- Abdel-Fattah MI, Tawfik AY (2015) 3D geometric modeling of the Abu Madi reservoirs and its implication on the gas development in Baltim area (Offshore Nile Delta, Egypt). *Int J Geophys* 2015:1–11
- Amoyedo S, Atoyebi H, Bally J, et al. (2016) Seismic-consistent reservoir facies modelling; a brownfield example from deep water niger delta. In: SPE Nigeria Annual International Conference and Exhibition. Paper presented at the SPE Nigeria Annual International Conference and Exhibition, Lagos, Nigeria, August 2016. Paper Number:SPE-184288-MS. <https://doi.org/10.2118/184288-MS>
- Asquith GB, Gibson CR (1982) Basic well log analysis for geologists. Amer assn of petroleum geologists
- Avseth P, Mukerji T, Mavko G (2010) Quantitative seismic interpretation: applying rock physics tools to reduce interpretation risk. Cambridge university press
- Ayodele OL (2019) An integrated study of the early cretaceous (valanginian) reservoir from the gamtoos basin, offshore south africa with special reference to seismic facies, formation evaluation and static reservoir modeling. Ph.D. Thesis, University of the Western Cape
- Ayodele O, Chatterjee T, Jvb D (2020) Seismic stratigraphic analyses of Early Cretaceous (Valanginian) sediments of Gamtoos Basin, offshore South Africa. *J Basic Appl Res Int* 26:1–14
- Ayodele OL, van Bever Donker JM (2016) Opuwari M (2016) Pore pressure prediction of some selected wells from the Southern Pletmos Basin, offshore South Africa. *S Afr J Geol* 119:203–214
- Bagheri M, Riahi MA, Hashemi H (2013) Reservoir lithofacies analysis using 3D seismic data in dissimilarity space. *J Geophys Eng* 10:035006
- Bohling G (2005) Stochastic simulation and reservoir modeling workflow. *Aust J Basic Appl Sci* 3:330–341
- Broad DS, Jungslager EHA, McLachlan IR, Roux J (2006) Offshore mesozoic basins. *Geol South Afr Geolo Soc South Afr Johannesburg/Council Geosci Pretoria* 553:571
- Calderon JE, Castagna J (2007) Porosity and lithologic estimation using rock physics and multi-attribute transform in Balcon Field, Colombia. *Lead Edge* 26:142–150
- Cannon S (2018) Reservoir modeling: a practical guide. Wiley
- Dake LP (1983) Fundamentals of reservoir engineering. Elsevier
- Elamri S, Opuwari M (2016) New Insights in the evaluation of reserves of selected wells of the pletmos basin Offshore South Africa. In: *SPE/AAPG Africa energy and technology conference*. OnePetro
- Eruteya OE, Dominick N, Moscariello A, Opuwari M (2018) Fluid escape above a gravity-driven linked system in the Orange Basin, Offshore South Africa. *AGU fall meeting abstracts*. pp S51E-0384
- Flint SS, Hodgson DM, Sprague AR et al (2011) Depositional architecture and sequence stratigraphy of the Karoo basin floor to shelf edge succession, Laingsburg depocentre, South Africa. *Marine Petrol Geol* 28:658–674
- Goovaerts P (1992) Factorial kriging analysis: a useful tool for exploring the structure of multivariate spatial soil information. *J Soil Sci* 43:597–619
- Hazlett RD (1997) Statistical characterization and stochastic modeling of pore networks in relation to fluid flow. *Math Geol* 29:801–822
- Kashif M, Cao Y, Yuan G et al (2019) Pore size distribution, their geometry and connectivity in deeply buried Paleogene Es1 sandstone reservoir, Nanpu Sag, East China. *Pet Sci* 16:981–1000
- Kyi KK, Dan HX, Najm E, Poh CH (2014) Carbonate reservoir facies and multi-pore system analysis using lwd resistivity imager acquired during pressurized mud cap drilling—a case study offshore Sarawak, Malaysia. In: *SPE Asia pacific oil & gas conference and exhibition*. OnePetro
- Larionov VV (1969) Borehole radiometry. Nedra, Moscow, p 127
- Levorsen AI, Berry FA (1967) Geology of petroleum. WH Freeman San Francisco
- Malan JA (1993) Geology, potential of Algoa, Gamtoos basins of South Africa. *Oil and gas journal*;(United States) 91:
- Mattar L, Dean L (2008) Reservoir engineering for geologists: part 6-well test interpretation. *Reservoir ISSUE* 4:
- McLean JK, Dulac JC, Gringarten E (2012) Integrated petrophysical uncertainty evaluation impacts reservoir models. *HART ENERGY, Exploration & Production*
- McMillan IK, Brink GI, Broad DS, Maier JJ (1997) Late Mesozoic sedimentary basins off the south coast of South Africa. *Sedimentary basins of the world*. Elsevier, pp 319–376
- Okoli AE, Agbasi OE, Lashin AA, Sen S (2021) Static reservoir modeling of the eocene clastic reservoirs in the Q-field, Niger Delta, Nigeria. *Nat Resour Res* 30:1411–1425
- Opuwari M (2010) Petrophysical evaluation of the Albian age gas bearing sandstone reservoirs of the OM field, Orange basin, South Africa. Ph.D. Thesis, University of the Western Cape
- Opuwari M, Mohammed S, Ile C (2021) Determination of reservoir flow units from core data: a case study of the lower cretaceous sandstone reservoirs, Western Bredasdorp Basin Offshore in South Africa. *Nat Resour Res* 30:411–430
- Pyrzcz MJ, Deutsch CV (2014) Geostatistical reservoir modeling. Oxford University Press

- Rahimi M, Riahi MA (2020) Static reservoir modeling using geostatistics method: a case study of the Sarvak Formation in an offshore oilfield. *Carbonates Evaporites* 35:1–13
- Soekor (1994) Licensing Round Information Brochure: Durban/Zulu-land Basin, Stellenbosch., p 24
- Spychala YT, Hodgson DM, Stevenson CJ, Flint SS (2017) Aggradational lobe fringes: The influence of subtle intrabasinal seabed topography on sediment gravity flow processes and lobe stacking patterns. *Sedimentology* 64:582–608
- Surpless KD, Ward RB, Graham SA (2009) Evolution and stratigraphic architecture of marine slope gully complexes: monterey Formation (Miocene), Gaviota Beach, California. *Mar Pet Geol* 26:269–288
- Thomson K (1999) Role of continental break-up, mantle plume development and fault reactivation in the evolution of the Gamtoos Basin, South Africa. *Mar Pet Geol* 16:409–429
- Viste I (2008) 3D modeling and simulation of multi-scale heterogeneities in fluvial reservoir analogues, Lourinhã Fm., Portugal: from virtual outcrops to process-oriented models. Ph.D. Thesis, MSc thesis, University of Bergen, Norway
- Worthington PF (1985) The evolution of shaly-sand concepts in reservoir evaluation. *The Log Analyst* 26:
- Yang T, Cao Y, Wang Y et al (2019) Determining permeability cut-off values for net pay study of a low-permeability clastic reservoir: a case study of the Dongying Sag, eastern China. *J Petrol Sci Eng* 178:262–271
- Yilmaz Ö (2001) Seismic data analysis: Processing, inversion, and interpretation of seismic data. Society of exploration geophysicists
- Yu X, Li X (2012) The application of sequential indicator simulation and sequential Gaussian simulation in modeling a case in Jilin Oilfield. Future control and automation. Springer, pp 111–118
- Zare A, Bagheri M, Ebadi M (2020) Reservoir facies and porosity modeling using seismic data and well logs by geostatistical simulation in an oil field. *Carbonates Evaporites* 35:1–10
- Zee Ma Y, La Pointe PR (2011) Uncertainty analysis and reservoir modeling: developing and managing assets in an uncertain world. AAPG, Tulsa, OK

Publisher's Note Springer Nature remains neutral with regard to jurisdictional claims in published maps and institutional affiliations.